The Heliosphere and Beyond

E. J. SMITH

Jet Propulsion Laboratory, California Institute of Technology, Pasadena, CA, USA

1. – Introduction

The concept of the heliosphere as a quasi-spherical cavity in the surrounding interstellar medium (ISM) has a history at least as long as that of an extended solar corona and solar wind [1, 2]. The concept originated in attempts to understand cosmic rays. Accumulating theoretical and observational evidence of a solar wind provided a natural explanation for the formation of this cavity and led to an examination of its structure. As spacecraft began to explore the heliosphere at increased radial distances, it became clear that the solar constituents inside the heliosphere and the interstellar constituents penetrating into the interior give rise to a wide range of dynamic phenomena including the acceleration of particles to high energies.

This lecture follows a logic similar to the first. It begins with a general discussion of the formation of the heliosphere and its interior and exterior structure. Following that, the major emphasis of the lecture is on two topics to which the recent Ulysses observations have made significant contributions. The first is the penetration of interstellar matter to within 5 AU of the sun, its interaction with the solar wind and the knowledge gained about the interstellar medium. The second topic addresses cosmic rays and particle acceleration inside the heliosphere especially in association with various types of collisionless shock. A brief description of the Ulysses mission was included in lecture I.

2. – The Heliosphere

Given the existence of the solar wind, important questions arise. How far does it extend into interstellar space? What is the nature of its interaction with the interstellar

medium?

As the solar wind dynamic pressure, nmV^2, falls off with increasing distance, it will eventually become equal to the pressure exerted inward by the surrounding interstellar medium. The distance at which this happens is poorly known because of difficulties in observing the various interstellar constituents. As a consequence, the distance to the solar - interstellar boundary is not known for certain with estimates ranging from ~80 - 150 AU.

The local interstellar medium is known to consist of some combination of dust, neutral gas, ionized plasma, magnetic fields and galactic cosmic rays. The inward pressure on the heliosphere is exerted by the interstellar plasma and magnetic field, the latter providing an identity that differs from the solar wind and its embedded magnetic field.

The best known interstellar component is the neutral gas (H, He) which enters the heliosphere more or less directly because it does not interact with the magnetic field in the solar wind. The neutral atoms then scatter short wavelength solar radiation, such as Lyman α, back into the inner heliosphere where it is observed by spacecraft orbiting above the Earth's atmosphere.

Diagnosis of such radiation has produced reasonably accurate values for the density, temperature and velocity of the interstellar hydrogen, the velocity showing that the interstellar medium has its own proper motion distinct from that attributable to the motion of the sun around the galactic center [3, 4, 5]. Unfortunately, the degree of ionization of the gas in interstellar space is too poorly known to infer the ion density. The magnetic field in the local interstellar medium or cloud is also unknown. Estimates of the ion density and field strength are available from astronomical observations but are always averages over much larger scales, comparable to the distance to the nearest stars, but not within 100 AU or so of the sun.

Irrespective of the scale involved, a reasonable physical model of the heliosphere has been developed. As in so many other cases, Eugene Parker was among the first to explore the consequences of the supersonic solar wind [2]. Figure 1, from his book, shows the velocity streamlines of the plasma inside and outside the heliosphere with the interstellar wind approaching from the right and the solar wind initially flowing radially outward from the sun. The interstellar plasma is seen to deflect around the heliosphere with an innermost streamline that splits near $\zeta = 1$ (the stagnation point). The solar wind must turn and flow tailward to exit the heliosphere and merge with the local ISM. Since its outward radial motion is supersonic, the solar wind must pass through a standing shock (shown) at which the directed flow is converted back into heat so that the subsonic plasma can be deflected and slide off parallel to the interstellar flow [6].

Another schematic representation of the heliosphere is shown in Figure 2 [7]. The outer boundary of the heliosphere (the heliopause) is shown along which the outward pressure of the solar wind and the inward pressure of the ISM are in balance. The radial solar wind flow passes through the egg-shaped Termination Shock, so-called because it terminates the supersonic solar wind flow. The subsonic flow "downstream" of the shock fills the cross-hatched region. The remaining feature is a possible bow shock in front of the heliosphere whose existence depends on whether the interstellar wind is supersonic.

The velocity of the plasma wind is "known", it is assumed to be equal to the velocity of the neutral gas, but the speeds of hydromagnetic waves, which depend on B, n and T, are not known. The Voyager spacecraft now approaching ~70 AU are expected to cross the Termination Shock, perhaps within the next few years, which will set the scale to the Heliopause and ISM and will provide an accurate estimate of the interstellar pressure.

The heliosphere itself is not the featureless "blob" represented by the empty region inside the Termination shock. Present are the solar wind electrons, protons and heavy ions, the solar-coronal magnetic field, energetic particles emitted by the sun and energetic particles accelerated inside the heliosphere as well as dust, all bathed in solar radiation, radio and plasma waves and solar x-rays. The solar wind itself exhibits considerable structure to be described briefly below. Overall, the heliosphere represents a plasma laboratory in which many different kinds of phenomena are accessible for study. In addition to the above, important constituents of interstellar space are able to penetrate deeply into the heliosphere where they interact with the solar wind. This aspect of heliospheric phenomena will now be discussed in some detail.

3. – Interstellar matter inside and outside the Heliosphere

The heliosphere is actually a semi-permeable body. The magnetized interstellar plasma is unable to enter this body but dust, neutral atoms and galactic cosmic rays (GCR) can cross the heliopause and penetrate deeply into the heliosphere (see Figure 3). Hydrogen atoms penetrate to within only ~5 AU of the sun before becoming ionized by short wavelength solar radiation or by giving up an electron to a solar wind ion (charge exchange). The atoms have so little mass that the inward force due to solar gravity is nearly compensated by the outward solar radiation pressure which increases the probability of ionization before the atoms reach the inner heliosphere. Neutral helium, on the other hand, being more massive and harder to ionize, can penetrate nearer the sun and has been detected at 1 AU [8].

The Ulysses spacecraft contains a unique instrument capable of detecting and counting the inflowing neutral helium atoms [9]. Because they interact only weakly with the heliosphere, and are largely unaffected by its interaction with the interstellar medium, the observations provide accurate estimates of the helium density and velocity in interstellar space[10]. The interstellar density is found to be $n(\mathrm{He}) = 1.7 \times 10^{-2}\mathrm{cm}^{-3}$ while the bulk velocity is 25 km/s coming from a direction whose galactic latitude and longitude are -5° and 74°, respectively. The average temperature is estimated to be $\approx$ 6500K.

Interstellar dust has also been detected, for the first time, by the Ulysses dust analyzer [11]. Figure 4 shows the good agreement found between model contours (panel B) and observations (panel A), during the first south polar passage [12]. The dust "hits" are shown as a function of time and the rotation angle of the spacecraft (relative to the ecliptic). (The geometry of the detector acceptance angles, the spacecraft spin axis and the direction to Earth is complex and they change as the spacecraft moves along a trajectory whose orbit plane is approximately perpendicular to the direction of the incoming dust.) Since the measurements were made at $\approx$ 5AU, the interstellar component

had to be distinguished from interplanetary dust (contributed by asteroids and comets) and from dust streams from Jupiter. In addition to direction of arrival, histograms of mass and impact speed were used to make this separation. The interstellar dust was then found to have a mean mass of 3×10^{-13} gm and a peak speed of $\approx$ 26 km/sec [13].

Comparison with the sizes of dust particles inferred from astronomical observations and dust models leads to a discrepancy with too many "massive" particles beyond a theoretical cutoff. However, the mass is still sufficiently low that the Lorenz force exerted on the electrically charged dust by the heliospheric magnetic field (HMF) dominates the force of solar gravity. The dust investigation has shown that interstellar dust is able to reach to within 1 AU of the sun.

Ulysses has also detected the interstellar atoms that become ionized and are convected outward in the solar wind (so called "pickup" ions) [14]. The pickup process leads to a velocity distribution for the ions which enables them to be readily distinguished from solar wind ions [15]. When the ion is created, it is essentially at rest in the inertial/spacecraft reference frame. It has a speed of only ~30 km/s as compared to the rapid motion of the solar wind past it at a speed, V_W, of 400-800 km/s. The ion senses the "frozen-in" HMF and begins to gyrate around the field with a speed V_W, which then corresponds to the temperature of the ions, i.e., they are very hot compared to the solar wind ion thermal speed.

The ion motion in the inertial frame consists of the resultant of the instantaneous gyro motion with circular velocity, $\mathbf{V_g}$, with $|\mathbf{V_g}| = V_W$, and the convected solar wind velocity, $\mathbf{V_W}$. When $\mathbf{V_g}$ is instantaneously aligned with the direction of the wind, the ion has velocity of $2V_W$. When $\mathbf{V_g}$ is opposite to the wind flow, the ion velocity is $\mathbf{V_g} - \mathbf{V_W} = 0$. Thus, the particle motion is a cycloid with velocity, $2V_W$, at the peaks and zero at the troughs.

Figure 5 shows the phase space distributions of H^+ and He^+ ions as a function of the ion speed normalized to the ambient wind speed. (The abscissa scale runs from 0.7 to 5 [14]. Obviously, ions with very low speeds are not detectable by the analyzer.) The flat distribution with a cutoff at $V/V_W = 2$ identifies these ions as interstellar in origin. (The instrument also detects solar wind protons which have been removed from the H^+ distribution, e.g., note the data gap near $V/V_W = 1$.)

These observations have provided information on (1) the ionization rates/scales of the interstellar neutrals, (2) the degree of coupling between the interstellar gas and the solar wind inside the heliosphere and (3) the densities of the neutrals in interstellar space before entering the heliosphere. The measured fluxes are consistent with a very long ionization scale length of ~1 AU (or ionization times of 3×10^5 seconds, i.e., several days). This parameter is not only of intrinsic interest but is needed to estimate the flux or density of neutrals outside the heliosphere.

The effect of ion pickup on the solar wind has long been a topic of keen interest [16]. In effect, the neutrals exert a drag force on the solar wind extending throughout much of the heliosphere. Their mass is being added to that of the solar wind, which is expected to slow down. At the same time, the interstellar ions are much hotter than the solar wind ions and can contribute heat to the solar wind causing an increase in temperature.

The two effects cause the solar wind flow to become less supersonic. A strong coupling of the solar wind "core" and the hot interstellar-ion "halo" could, in principle, reduce the flow to being subsonic before reaching the heliopause, in which case a termination shock would not occur.

The physical mechanism that could couple the two fluid components is a collisionless wave-particle instability [17, 18]. If the ions were to be picked up in a quiet magnetic field or over a short range of distances, their initial pitch angle distribution (the angles between the ion velocities, $\mathbf{V}$, and the magnetic field direction $\mathbf{B}$) could take the asymmetric form of a ring (for a field orientation perpendicular to the flow) or a beam (for a field parallel to the flow). Ion cyclotron waves would then be excited which would scatter the particles in pitch angle to form a spherically symmetrical stable distribution. The waves could also transfer energy (heat) from the interstellar ions to the solar wind ions.

The ion cyclotron waves predicted by this instability have, in fact, been observed in Ulysses magnetic field data (see Figure 6) [19]. The magnetic field spectra show sharp increases at and above the proton gyro frequency (dashed vertical line) consistent with theory. The waveforms associated with the waves are also visible in the data as shown in one of the panels. However, the waves have been found to occur only intermittently (when the field tends to be parallel to the flow, unlike the Parker spiral at large heliodistances) and are weak when they do occur. The explanation appears to be that the pickup ions are created over such a large distance scale ($\sim$1 AU as above) that the variable field direction has virtually all orientations and the initial pitch angle distribution tends to be spherically symmetrical already, so the ion cyclotron instability is weak [20]. Thus, there appears to be only a weak coupling between the two fluids and the interstellar ions may persist as a separate component throughout the heliosphere.

In order to estimate the flux and density of neutrals in interstellar space from the density of pickup ions inside the heliosphere within $\sim$5 AU of the sun, allowance must be made for various effects. The principal effect is the rate of ionization which can be inferred in the region of observation but which varies with radial distance in the outer heliosphere as both the intensity of solar radiation and the density of solar wind ions available for charge exchange decrease. Available theory is used to model the decrease in ionization rate or scale.

After allowance for this effect, the pickup measurements lead to estimates of the neutral gas densities at the location of the temination shock [14]. The inferred hydrogen density, $n(\mathrm{H}) = 0.125 \pm 0.015\mathrm{cm}^{-3}$, the helium density, $n(\mathrm{HeI}) = 0.0155 \pm 0.0015$ and their ratio is then 8.1 ± 1.3. The latter can be compared with the "standard universal" abundance ratio of 10.

In the case of hydrogen, the most abundant element of the interstellar gas, an adjustment must also be made to infer correctly the neutral flux incident on the heliosphere. The physical effect is a slowing of the hydrogen in interstellar space just outside the heliosphere by a process called "filtration" [21]. Whether an interstellar bow shock exists or not, the interstellar plasma is forced to divert around the heliosphere with an accompanying change in its velocity relative to the interstellar neutrals.

Well upstream of the heliopause, the neutrals are assumed to have the same speed

as the plasma. As the interstellar ions are slowed by their approach to the heliopause, they are overtaken by the neutrals which are not affected initially. Charge exchange will occur with electrons being transferred from the faster neutrals to the slower ions to yield a slower neutral. Filtration is an efficient process made evident by the measured differences in the speeds of the hydrogen (inferred from back scattered Lyman radiation as 20 km/s) and helium as measured by the Ulysses neutral particle detector (25 km/s).

The effect of filtration depends on several parameters: the width of the filtration region, taken to be 140 ± 40 AU, the proton-hydrogen charge exchange cross section ($5.3 \times 10^{-15} \mathrm{cm}^2$) and the average speed between the protons and the hydrogen, 19 km/sec. The filtration factor derived on the basis of these parameters equals 0.58. The inferred hydrogen density in the local interstellar cloud is then N(H) = 0.20 cm^{-3} while the helium density is unchanged so that N(HeI) = 0.0155 cm^{-3}. Their ratio is then 13/1.

Knowledge of the neutral densities also leads to estimates of the ion densities in the local interstellar cloud (LISC). The ion densities depend on knowledge of the fraction of neutrals that are ionized. This fraction is typically not well known although limits exist based on astronomical observations and theory. The fraction is thought to be reasonably well known for hydrogen with a value of 0.18 so that $\mathrm{N(H^+)} = \mathrm{N}_T\mathrm{(H)} - \mathrm{N(H)} = 0.18\ \mathrm{N}_T\mathrm{(H)}$. Solving this equation yields an estimate of the total amount of interstellar hydrogen, $\mathrm{N}_T\mathrm{(H)} = 0.243\ \mathrm{cm}^{-3}$. If one assumes the solar system abundance ratio of H/He = 10 applies to the sums of the neutral and ion densities, the fraction of helium atoms ionized, f, can be estimated from $0.243/0.0155(1+f) = 10$. This approach leads to $f = 0.59$ and to $\mathrm{N(He^+)} = 0.0090\ \mathrm{cm}^{-3}$.

The ion densities can be used to estimate the plasma pressure in the interstellar medium assuming a temperature, e.g., the same as that of the interstellar neutrals (7000 K), i.e., thermal equilibrium. The other component of interstellar pressure contributed by the magnetic field can then be estimated from the size of the heliosphere and a value for the field magnitude derived [22].

Figure 7 combines information of these various parameters all related to size of the heliosphere. The x axis shows the distance to the termination shock with 80-90 AU (the gray bar) designated as the likely range of distances within which it is located (based on inferences drawn from the changing intensity and spectrum of Anomalous Cosmic Rays which are discussed below) [23]. The lower half-figure contains the fractional ionization of H and He with higher degrees of ionization corresponding to locations of the termination shock nearer the sun. The total electron density, n_e, is also shown as derived from the H, He ionization.

The upper half-figure contains information about the interstellar field. For an average solar wind pressure varying as r^{-2} (constant speed), and an assumed ratio of the pressures upstream and downstream of the termination shock, the total pressure, $2nkT + B^2/8\pi$, can be inferred as a function of the shock location. Then, using the information on ion/electron density, the pressure to be supplied by the field can be calculated. The result is shown in the figure as ranging between 0.8 and 2.0 μGauss (80 - 200 pT). The upper and lower curves and the horizontal bar denote the estimated uncertainty in $|B|$ and the current best estimate of the interstellar field magnitude based on astronomical

observations. This calculation shows that the various interstellar parameters derived in this way are reasonably consistent with other lines of evidence.

4. – Galactic Cosmic Rays

The cosmic rays entering the heliosphere are accelerated elsewhere in the galaxy to velocities approaching the speed of light. They include heavy elements, all of whose electrons have been stripped off leaving a bare nucleus. It is customary to express their energy in terms of energy per nucleon rather than total energy. Their gyro-radii in the weak interstellar and distant heliospheric magnetic fields are sufficiently large that they are expected to cross the heliopause easily.

However, once inside the heliosphere, various effects combine to oppose their further penetration and only an unknown fraction are able to reach the inner heliosphere. In particular, the lowest energy particles beginning at < 1 GeV are strongly affected and observed energy spectra cannot be inverted to derive their spectra before they arrive at the heliosphere. A further complication is the time dependence of the structure and dynamics of the heliosphere which produces a "modulation" of the cosmic rays over the sunspot cycle.

Figure 8 illustrates several of the above comments. The differential intensity, i.e., the flux ($m^{-2}s^{-1}$) per unit energy interval (MeV) and unit solid angle (steradians), is shown for protons as a function of total kinetic energy [24]. Four of these energy spectra are shown for different phases of the solar cycle from minimum (1965) to maximum (1972). The decrease in intensity below ~300 MeV represents both a decrease in flux and a loss of energy for those particles able to penetrate to within an AU of the Sun. Fewer particles are able to reach the interior when the sun is active.

The physical effects which transform the galactic cosmic rays are all associated with the presence of the heliospheric magnetic field. Theorists have developed the transport equation governing the behavior of the cosmic rays [25, 26].

$$\begin{aligned}
\frac{\partial f}{\partial t} = & \frac{\partial}{\partial x_i}\left[k_{ij}\frac{\partial f}{\partial x_j}\right] && \textit{(diffusion)} \\
& - U_i \frac{\partial f}{\partial x_i} && \textit{(convection)} \\
& - V_{d,i}\frac{\partial f}{\partial x_i} && \textit{(guiding - center drift)} \\
& + \frac{1}{3}\frac{\partial U_i}{\partial x_i}\left[\frac{\partial f}{\partial \ln p}\right] && \textit{(energy change)} \\
& + Q(x_i, t, p) && \textit{(source)}
\end{aligned}$$

The distribution function, f, is the result of four effects as indicated. As discussed earlier, the heliospheric magnetic field is not smooth but varies in direction and to a lesser extent in magnitude on essentially all time scales. Many of these changes are sufficiently rapid (seconds to minutes) as to constitute discontinuities in the field. (There are two

common types, rotational and tangential discontinuities, although it is not always easy to distinguish between them operationally.) These irregularities scatter the cosmic rays, simply by altering their pitch angles, so that they effectively undergo a random walk along and across field lines. This effect is most economically described in terms of an inward anisotropic diffusion of the cosmic rays indicated by the first term on the right-hand side of the transport equation. The second term represents outward convection of the cosmic rays caused by the presence of the solar wind **E** field ($\mathbf{E} = -\mathbf{V} \times \mathbf{B}$ in inertial space).

The smooth global or background magnetic field, represented by the Parker spiral field, affects the cosmic rays by contributing drift motions associated with the gradients in field magnitude, the curvature of the field and any abrupt changes in field direction (as at the current sheet). An example of these drifts is shown in Figure 9 for protons of a specific energy (2 GeV) and the phase of the solar magnetic cycle in which the field is outward in the north polar cap (designated as $qA > 0$) [27]. The dashed lines are locii showing the protons entering the heliosphere over the poles and exiting along the equator. The heavy wavy curve represents drift along the heliospheric current sheet which dominates the equatorial motion. Thus, the cosmic rays circulate from outside to inside and back outside the heliosphere in the form of a quasi-stationary flow.

A physical model that explains the drift of cosmic rays along the current sheet is shown in Figure 10 [28]. The magnetic field is outward above and inward below the current sheet as indicated by the circles enclosing the dots and crosses. The wavy lines are streamlines of positively charged particles which gyrate around outward fields in a clockwise sense above the current sheet and around inward fields in a counter clockwise sense below the current sheet. The net effect is a drift along the current sheet (in the direction of the current flow).

Prior to the Ulysses mission, it was believed possible that cosmic rays preferentially entered the heliosphere from above the Sun's poles. Qualitatively, the fields over the poles could form a "funnel" allowing easy access of the cosmic rays compared to the long paths along fluctuating spiral fields in and near the equator. Using values of the diffusion coefficients parallel and perpendicular to **B** appropriate to observations in the equatorial heliosphere, theory predicted a large increase in intensity at high latitude by a factor of $\sim$3 for relatively low energies and $\sim$1.6 for higher energies (see Figure 11). In fact, the Ulysses data (also shown in Figure 11) showed essentially no change at low energies and an increase by about 30% at high energies [29].

This rather surprising result was readily explained by the Ulysses magnetic field measurements. It was shown in Part I that the fast high latitude solar wind contains persistent large amplitude Alfvén waves (or long period "stochastic variations") [30]. The waves cover a broad range of frequencies that include the gyro frequencies of the relativistic cosmic rays implying that the particles will be scattered back into the outer heliosphere very effectively. The importance of such field irregularities in preventing easy cosmic ray access over the poles had been predicted on the basis of the random walk of the fields commonly observed in association with convective (granular and supergranular) motions in the solar photosphere [31].

5. – Anomalous Cosmic Rays

A species of cosmic ray was identified several decades ago and designated as anomalous on the basis of the relative abundances which were very unlike the galactic cosmic rays [32, 33, 34]. An early postulate which has survived various tests ever since is that the composition is governed by hard-to-ionize neutral atoms that can propagate over large distances in the galaxy but become ionized upon entering the heliosphere [35]. Another distinction of the anomalous cosmic rays (ACR) is that they are singly ionized, like most pickup ions, and are not fully ionized like the galactic cosmic rays. Finally, anomalous cosmic rays occupy an energy range of tens of MeV per nucleon, intermediate between the lower energy solar particles and galactic cosmic rays. For a representative energy spectrum see Figure 12 [47].

The acceleration inside the heliosphere to such high energies of what are essentially pickup ions has excited considerable interest and has led to a generally accepted interpretation. A model that attributes their acceleration to drift motion along the termination shock (shock drift acceleration) has had considerable success [36]. According to this view, once created, the ions are transported by the solar wind outward to the termination shock, acquire high energies and are then able to diffuse back into the inner heliosphere where they are observed. The anomalous cosmic rays exhibit solar modulation, having a maximum intensity at solar minimum and a decreased intensity or disappearance at solar maximum, qualitatively similar to the variations in the galactic cosmic rays.

Shock drift acceleration has successfully explained the total energy available to the anomalous cosmic rays while detailed modeling is able to reproduce the observed energy spectra. A simple calculation illustrates the energy gain based on the voltage available to a particle drifting from the equator to the pole along the heliospheric electric field. As shown in Part I, the north-south electric field associated with the solar wind is $E_\theta = -V \times B = V_r B_\phi$. The Parker model for the spiral field implies $B_\phi = -\Omega \sin\theta \, B_{r_0} r_0^2 / r V_r$. Written in terms of the radial field and distance at 1 AU, represented by subscript zero, $E_\theta = -\Omega \sin\theta \, B_{r_0} r_0^2 / r$.

The voltage from equator to pole is then is $\int_{\pi/2}^{0} E_\theta r \, d\theta = -\Omega \, r_0^2 B_{r_0}$. Substituting representative values of the parameters, V = (400 km/s) (3×10^{-9}T) (1.5×10^{11} m) $= 2 \times 10^8$ volts. Therefore, 200 MV are available, in principle, to accelerate the particles.

Figure 13 shows the spectral intensities of H^+, He^+, O^+ as a function of total energy in MeV. The notable feature is the broad maxima in each case around 100 - 200 MeV, consistent with the above calculation [26].

Ulysses experiments regularly observe anomalous cosmic rays and their latitude gradient, like that of the galactic cosmic rays, was of interest. Figure 14 shows typical results for oxygen from 8 - 12 MeV/nucleon (upper panel) and 12-16 MeV/nucleon (lower panel) as a function of colatitude, θ [37]. The y axis consists of the ratio of anomalous cosmic ray fluxes as observed at Sampex (a spacecraft in orbit around Earth) and at Ulysses. This ratio was formed in order to cope with the time dependent variation associated with solar modulation while the latitude ranges were being transversed. The latitude gradients are seen to be $\sim$ 2%/degree at both energies, i.e., about an order of magnitude

larger than the gradient found for GCR with energies of approximately 1 GeV.

6. – Brief Summary of other important Ulysses results

Time and space have not permitted a detailed discussion of other important results obtained by the Ulysses mission. In the context of this discussion of the heliosphere and beyond, it would have been desirable to include the major findings regarding the internal structure of the inner heliosphere imposed by solar wind variations. Much effort has been devoted to studying the two largest scale structures inside the heliosphere at low latitudes, namely, corotating interaction regions/CIRs and the adjacent corotating rarefaction regions/CRRs caused by the alternating fast and slow solar wind streams. Of particular interest is the formation of shocks beyond ~2 AU which are effective in accelerating particles, presumably from the superthermal tail of the solar wind distribution, to ~MeV energies.

There are two types of shock, a "forward" shock propagating outward in the solar wind (at ~100 km sec^{-1}) and a "reverse" shock propagating sunward but convected outward by the more rapid motion of the solar wind. At low latitudes, where they are observed, the forward shocks have been shown to be propagating equatorward and westward while the reverse shocks are propagating polarward and eastward in solar coordinates [38]. These directions of propagation are consistent with a 3D model of the interactive regions based on a simple tilted dipole configuration with a slow equatorial wind and fast higher latitude wind [39].

Surprisingly, the shock accelerated particles have been found at higher latitudes than are reached by the CIRs or their associated shocks [40]. Two explanations have been offered. One involves enhanced diffusion of the particles across field lines because of the large amplitude fluctuations in the magnetic field typically found at much higher latitudes [41]. The other explanation involves a new model of the HMF that includes several features ignored in the earlier Parker model, namely the non-radial expansion of the field and wind from the poles, the outflow of the wind from polar coronal holes and the differential rotation of the photospheric field (variation of angular velocity with latitude) [42].

Another unexpected surprise has been evidence of a north-south asymmetry in the heliosphere. This asymmetry was first seen in the GCR which revealed the same latitude gradients in the north and south hemispheres but with a higher intensity in the north equivalent to a displacement of the heliospheric equator southward by ~10° [43, 44]. The anomalous cosmic ray observations, although exhibiting a larger latitude gradient as mentioned above, also showed the same north/south asymmetry. It would be expected that a corresponding asymmetry would exist in the heliomagnetic field measurements. If the north and south heliosphere occupy different volumes but contain the same magnetic flux, a difference in the values of B_r might be expected with larger values in the south (the smaller semi-heliosphere) than in the north.

The initial search for such a magnetic field asymmetry was unsuccessful [45], in retrospect, because of a time variation in B that developed while the spacecraft was traveling

from 80° south to 80° north. Simultaneous observations by the WIND spacecraft in the ecliptic during the same interval revealed a difference in B_r in the positive and negative magnetic sectors that is consistent with a 10° southward displacement of the HCS and, thus, with the energetic particle results [46]. Such an asymmetry has important implications for the Sun's polar magnetic field strength and other conditions in the sun's polar regions.

There have also been a number of Ulysses observations that have astrophysical implications. Measurements of GCR isotopes have provided information on the lifetimes of the cosmic rays within the galaxy and information on the nucleosynthesis involved in their production [48]. The abundance of ^{3}He in interstellar space has implications for the Big Bang scenario and for the early baryon content of the Universe [49].

Fortunately, many discussions of these and other topics that may be of interest to the reader can be found in special issues of various U.S. and European journals devoted to the Ulysses results.

Continuation of the Ulysses mission has been approved by NASA and ESA through the coming solar maximum where, once again, the spacecraft will sample the high latitude heliosphere but under drastically different conditions than during solar minimum. Thus, we can anticipate learning a lot more of scientific interest from Ulysses during the coming years.

* * *

The invitation to attend the meeting and the support provided by the Italian Physical Society are greatly appreciated. The assistance of Joyce Wolf was once again indispensable. Neil Murphy supplied the previously unpublished Figure 6. Portions of this report present work done at the Jet Propulsion Laboratory of the California Institute of Technology for the National Aeronautics and Space Administration.

REFERENCES

[1] DAVIS L.,*Phys.Rev.*, **100** (1955) 1440.
[2] PARKER E. N., *Interplanetary Dynamical Processes* (Interscience, New York) 1963.
[3] THOMAS G. E. and KRASSA R. F., *Astron. Astrophys.*, **11** (1971) 11,218.
[4] BERTAUX J. L., LALLEMENT R., KURT V. G. and MIRONOVA E. N., *Astron.Astrophys.*, **150** (1985) 1.
[5] GEISS J. and WITTE M., *Space Science Reviews*, **78** (1996) 229.
[6] CLAUSER F., *4th Symposium on Cosmical Gas Dynamics*, (Varenna, Italy) 1960.
[7] AXFORD W. I, in *Physics of the Outer Heliosphere*, edited by S. GRZEDZIELSKI and D. E. PAGE (Pergamon Press, Oxford) 1990, pp. 7-19.
[8] MOEBIUS E. *et al.*, *Nature*, **318** (1985) 426.
[9] WITTE M. *et al.*, *Astron.Astrophys.*, **92** (1992) 333.
[10] WITTE M., BANASZKIEWICZ M., and ROSENBAUER H., *Space Science Reviews*, **78** (1996) 289.
[11] GRUEN E. *et al.*, *Astron. Astrophys.*, **92** (1992) 411.
[12] BAGUHL M., HAMILTON D. P., GRUEN E., *et al.*, *Science*, **268** (1995) 1016.

[13] GRUEN E., GUSTAFSON B., MANN I., MORFILL G. E., STAUBACH P., TAYLOR A., and ZOOK H. A., *Astron. Astrophys.*, **286** (1994) 915.
[14] GLOECKLER G., *Space Science Reviews*, **78** (1996) 335.
[15] VASYLIUNAS V. M. and SISCOE G. L., *J. Geophys. Res.*, **81** (1976) 1247.
[16] HOLZER T. E., *Ann. Rev. Astr. Astrophys.*, **27** (1989) 199.
[17] WU C. S. and DAVIDSON R. C., *J. Geophys. Res.*, **77** (1972) 5399.
[18] LEE M. A. and IP W.-H., *J. Geophys. Res.*, **92** (1987) 11041.
[19] MURPHY N., SMITH E. J., TSURUTANI B. T., BALOGH A., and SOUTHWOOD D. J., *Space Science Reviews*, **72** (1994) 447.
[20] ISENBERG P. A., in *Solar Wind Eight*, edited by D. WINTERHALTER, J. T. GOSLING, S. R. HABBAL, W. S. KURTH, M. NEUGEBAUER, (American Institute of Physics, Woodbury) 1996, pp. 626-629.
[21] BARANOV V. B. and MALAMA Y. G., *J.Geophys. Res.*, **100** (1995) 755.
[22] GLOECKLER G., FISK L. A., and GEISS J., *Nature*, **386** (1997) 374.
[23] STONE E. C., CUMMINGS A. C. and WEBBER W. R., *J. Geophys. Res.*, **101** (1996) 11,017.
[24] FISK L. A., in *Solar system plasma physics* edited by E. N. PARKER, C. F. KENNEL, and L. J. LANZEROTTI (North Holland, Amsterdam) 1979, vol. 1, pp. 179-247.
[25] PARKER E. N., *Planet. Space Sci.*, **13** (1965) 9.
[26] JOKIPII J. R., in *Physics of the outer heliosphere*, edited by S. GRZEDZIELSKI and D. E. PAGE, (Pergamon Press, Oxford) 1990, pp. 169-178.
[27] JOKIPII J. R., in *Cosmic winds and the heliosphere*, edited by J. R. JOKIPII, C. P. SONETT, and M. S. GIAMPAPA, (Univ. of Arizona press, Tucson) 1997, pp. 833-855.
[28] JOKIPII J. R., LEVY E. H., and HUBBARD W. B., *Astrophys. J.*, **213** (1977) 861.
[29] SIMPSON J. A. *et al.*, *Science*, **268** (1995) 1019.
[30] SMITH E. J., BALOGH A., NEUGEBAUER M., and MCCOMAS D., *Geophys. Res. Lett.*, **22** (1995) 3381.
[31] JOKIPII J. R. and KÓTA J., *Geophys. Res. Lett.*, **16** (1989) 1.
[32] GARCIA-MUNOZ M., MASON G. M., and SIMPSON J. A., *Astrophys. J. Letters*, **182** (1973) L81.
[33] HOVESTADT D., VOLLMER O., GLOECKLER G., and FAN C. Y., *Phys. Rev. Letters*, **31** (1973) 650.
[34] MCDONALD F. M., TEEGARDEN B. J., TRAINOR J. H., and WEBBER W. R., *Astrophys. J. Letters*, **187** (1974) L105.
[35] FISK L. A., KOZLOVSKY B., and RAMATY R., *Astrophys. J. Letters*, **190** (1974) L35.
[36] PESSES M. E.,. JOKIPII J. R, and EICHLER D., *Astrophys. J. Letters*, **246** (1981) L85.
[37] TRATTNER K. J. *et al.*, *Geophys. Res. Lett.*, **22** (1995) 3349.
[38] GOSLING J. T. *et al.*, *Geophys. Res. Lett.*, **22** (1995) 3333.
[39] PIZZO V. J., *J. Geophys. Res.*, **96** (1991) 5405.
[40] SIMNETT G. M. *et al.*, *Space Science Reviews*, **83** (1998) 215.
[41] KÓTA J. and JOKIPII J. R., *Science*, **268** (1995) 1024.
[42] FISK L., *J. Geophys. Res.*, **101** (1996) 15,547.
[43] SIMPSON J. A., ZHANG M., and BAME S., *Astrophys. J.*, **465** (1996) L69.
[44] HEBER B., DROEGE W., FERRANDO P. *et al.*, *Astron. Astrophys.*, **316** (1996) 538.
[45] ERDÖS G. and BALOGH A., *Geophys. Res. Lett.*, **25** (1998) 245.
[46] SMITH E. J., JOKIPII J. R., KÓTA J., LEPPING R. P., and SZABO A., to appear in *Astrophys. J.*, 1999.
[47] GLOECKLER G., *Revs. Geophys. Space Phys.*, **17** (1979) 569.
[48] SIMPSON J. A. and CONNELL J. J., *Astrophys. J. Letters*, **497** (1998) L85.
[49] GLOECKLER G. and GEISS J., *Nature*, **381** (1996) 210.

Fig. 1. Velocity streamlines inside and outside the heliosphere [2]. The interstellar wind approaches from the right and is deflected around the cavity formed by the solar wind, the heliosphere. The sun is located at the origin of the coordinate system. The diverging radial lines near the sun represent the outward flow of the solar wind. In the outer heliosphere the solar wind turns to become parallel to the interstellar wind and exits through an extended open tail.

Fig. 2. Schematic representation of the heliosphere showing additional external and internal structure [7]. The interstellar wind is assumed to be supersonic so that a shock wave develops in front of the heliosphere across which the magnetized plasma component is deflected abruptly. The outer boundary of the heliosphere, the heliopause, is delineated by the crosshatched subsonic solar wind inside the heliosphere. The inner egg-shaped contour represents the Termination Shock across which the radially diverging supersonic solar wind undergoes an abrupt transition to subsonic flow.

Fig. 3. Schematic showing neutrals and cosmic rays entering the heliosphere. The heliosphere is shown with the sun at its center and a field line spiraling outward. Three trajectories are shown, two for neutral atoms and the other for a cosmic ray. The lower of the neutral trajectories shows the atom becoming ionized inside the heliosphere and picked up by the solar wind to be transported outward. The cosmic ray is affected by the heliospheric magnetic field and follows the field inward while being scattered by field irregularities.

Fig. 4. Detection of interstellar dust [11]. Both panels are plots of spacecraft rotation angle versus time. Panel B contains contours of the flux of interstellar dust based on arrival at the heliosphere with the same direction and velocity as the neutral interstellar gas. Panel A shows the directions of arrival of dust particles detected by the dust analyzer. There is an obvious correspondence.

Fig. 5. Detection of hydrogen and helium pickup ions [14]. Two phase space densities are shown as a function of the ratio of the ion speed to the solar wind speed. The contributions of solar wind protons and alpha particles have been removed so only the interstellar pickup ions are shown. The characteristic feature of pickup ions is the abrupt cutoff at ion speed /wind speed = 2.

Fig. 6. Observations of ion cyclotron waves associated with pick up protons. This figure contains four power spectra and a plot of the three field components and field magnitude. The data were transformed into coordinates parallel and perpendicular to the average field direction before analysis. The spectra are cross spectra containing a sloping line corresponding to a least squares fit to the whole data set. The vertical dotted lines correspond to various ion gyro frequencies, the highest being the proton gyro frequency. The characteristic feature of pickup ion waves is the sharp onset at the proton gyro frequency and wave power above that frequency as is seen. The panel on the lower right contains the waveforms.

Fig. 7. Magnetic field and electron density in Local Interstellar cloud [22]. The various interstellar parameters are plotted as a function of the heliospheric distance to the termination shock, which basically sets the scale of the heliosphere. The upper panel shows the inferred variation in magnetic field magnitude with distance to the shock

based on a model described in the text, which balances the interior and exterior plasma pressures. The solid line represents the best estimate and the dashed lines are confidence limits. The dark horizontal bar indicates the probable value of B inferred by other means. The lower panel contains two curves representing the fractional ionization of hydrogen and helium. The lower curve is the inferred interstellar electron density.

Fig. 8. Intensity of cosmic rays at different phases of solar activity [24]. Energy spectra of cosmic ray protons are shown as a function of kinetic energy. The ordinate is differential intensity. The turnover at several hundred MeV shows the effect of the heliosphere on the spectrum which probably continues to increase with energy in interstellar space. The effect of solar activity and the heliosphere on cosmic rays is evident in the decrease in intensity at low energies during maximum solar activity (1969).

Fig. 9. Drift patterns of cosmic rays in the heliospheric magnetic field [26]. The changing magnitude and curvature of the global magnetic field cause incoming cosmic rays to execute drifts as indicated by the dashed contours. The solid wavy curve is the heliospheric current sheet along which the particles exit the heliosphere. Overall, there is a circulation of the cosmic rays from inward over the poles and out along the current sheet. This condition is for positive magnetic polarity of the heliospheric field in the north polar cap. In the alternate sunspot cycle, the field will be negative (inward) in the north polar cap and the direction of the drifts will be reversed.

Fig. 10. Drift of cosmic rays along the current sheet [28]. The dots and crosses inside the circles represent the direction of the magnetic field (outward above, inward below the current sheet). The wavy curves represent the drift of two sample particles along the current sheet. The basic motion is outward in the same direction as the current in the current sheet. The motion of the particles is clockwise around outward fields then, as the particle crosses the current sheet, the sense of rotation reverses and the particle proceeds outward along the current sheet.

Fig. 11. Observed cosmic ray measurements compared with theory [29]. Ulysses measurements of cosmic ray intensities are shown as a function of time with latitude along the top scale. The interval covered extends from the time the spacecraft left the ecliptic until it returned after having passed under the sun and the South Pole. The two panels represent measurements at different energies with higher energies in the lower panel. The flux measurements have been normalized to simultaneous measurements in the ecliptic by the IMP spacecraft in order to guard against time/ solar modulation, i.e., solar cycle, variations. The dotted curves are theoretical values based on a standard model and, as can be seen, predict a large increase with increasing latitude in contrast to the observations. These results show that entry of cosmic rays over the poles is not as preferred as anticipated in the model.

Fig. 12. Energy spectrum showing the presence of Anomalous Cosmic Rays superposed on the Galactic Cosmic Ray spectrum [47]. Spectra are shown for several of the dominant elements of anomalous cosmic rays. They are a composite of measurements by several research groups (as indicated by different symbols) which each cover different energy ranges as determined by the instrumentation used. The ACR produce a "bump" in the cosmic ray spectrum at tens of MeV and lie between the lower energy energetic

solar particles and the higher energy galactic cosmic rays.

Fig. 13. Energy spectra of anomalous cosmic rays as a function of total energy [26]. It is customary, as in Figure 12, to plot spectra as a function of energy per nucleon which emphasizes the similarities and differences between different species. This plot, however, shows the intensities of hydrogen, helium and oxygen as a function of total energy. There is more hydrogen than helium and more helium than oxygen, as expected, although the relative abundances differ significantly from the standard universal compositions. There is an obvious correspondence in that the particles have been accelerated to similar energies in spite of their different masses. It is noteworthy that the ACR are predominantly singly charged instead of completely stripped of electrons like the GCR, the reason being that they are neutrals that become ionized inside the heliosphere.

Fig. 14. Latitude gradient of anomalous cosmic rays [37]. The two panels reveal the latitude gradients for oxygen at two different energies, 8-12 MeV/ nucleon in the upper figure and 12- 16 MeV/ nucleon in the lower panel. The ratio of fluxes at the inecliptic spacecraft, SAMPEX, designated S, and at Ulysses, U, are shown as a function of latitude. The ratio is taken in order to correct for solar cycle modulation which causes a significant time variation during the measurement interval. The data are plotted as a function of colatitude, θ, rather than as a function of latitude. The latitude gradient is approximately 2%/ deg (a factor of about 10 larger than for high energy galactic cosmic rays), is increasing toward the pole and is larger at lower energies. Previous measurements over a more limited latitude range have shown that the sign of the gradient reverses when the sun's polar cap magnetic field changes sign near solar maximum.

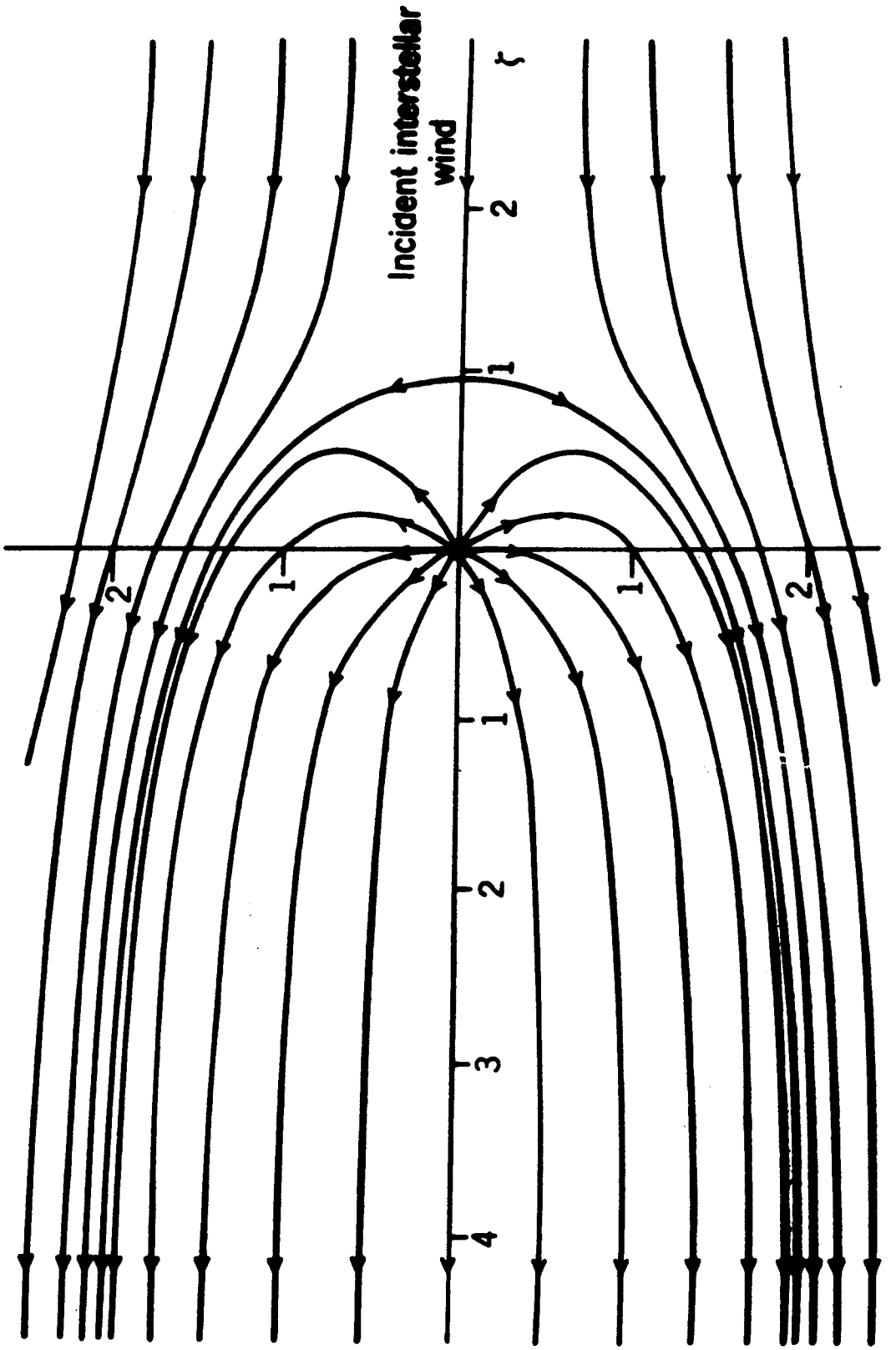
Incident interstellar wind
ζ
2
1
1
2
1
1
2
3
4

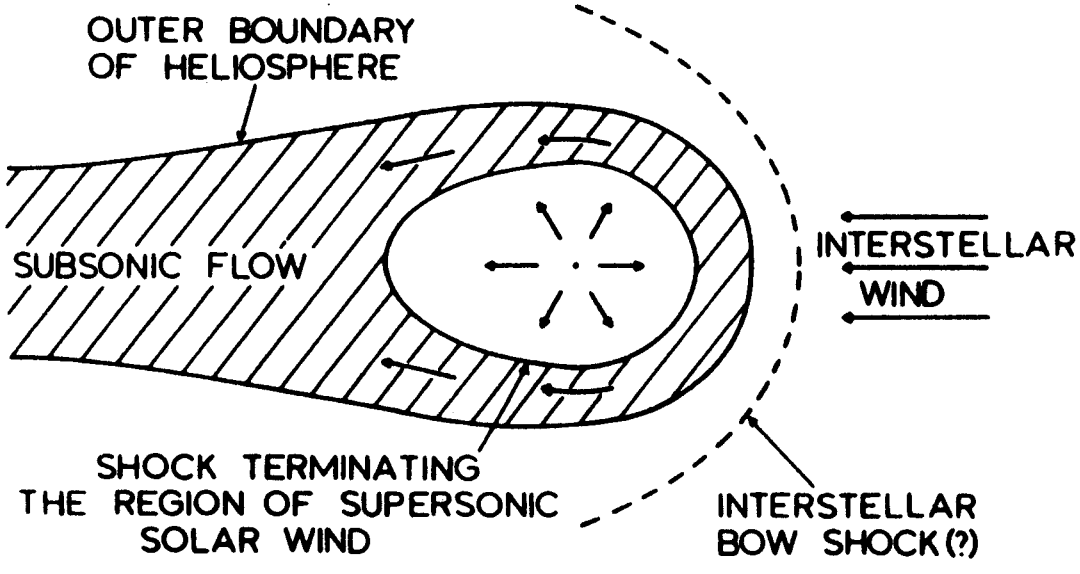
OUTER BOUNDARY
OF HELIOSPHERE
SUBSONIC FLOW
INTERSTELLAR
WIND
SHOCK TERMINATING
THE REGION OF SUPERSONIC
SOLAR WIND
INTERSTELLAR
BOW SHOCK(?)

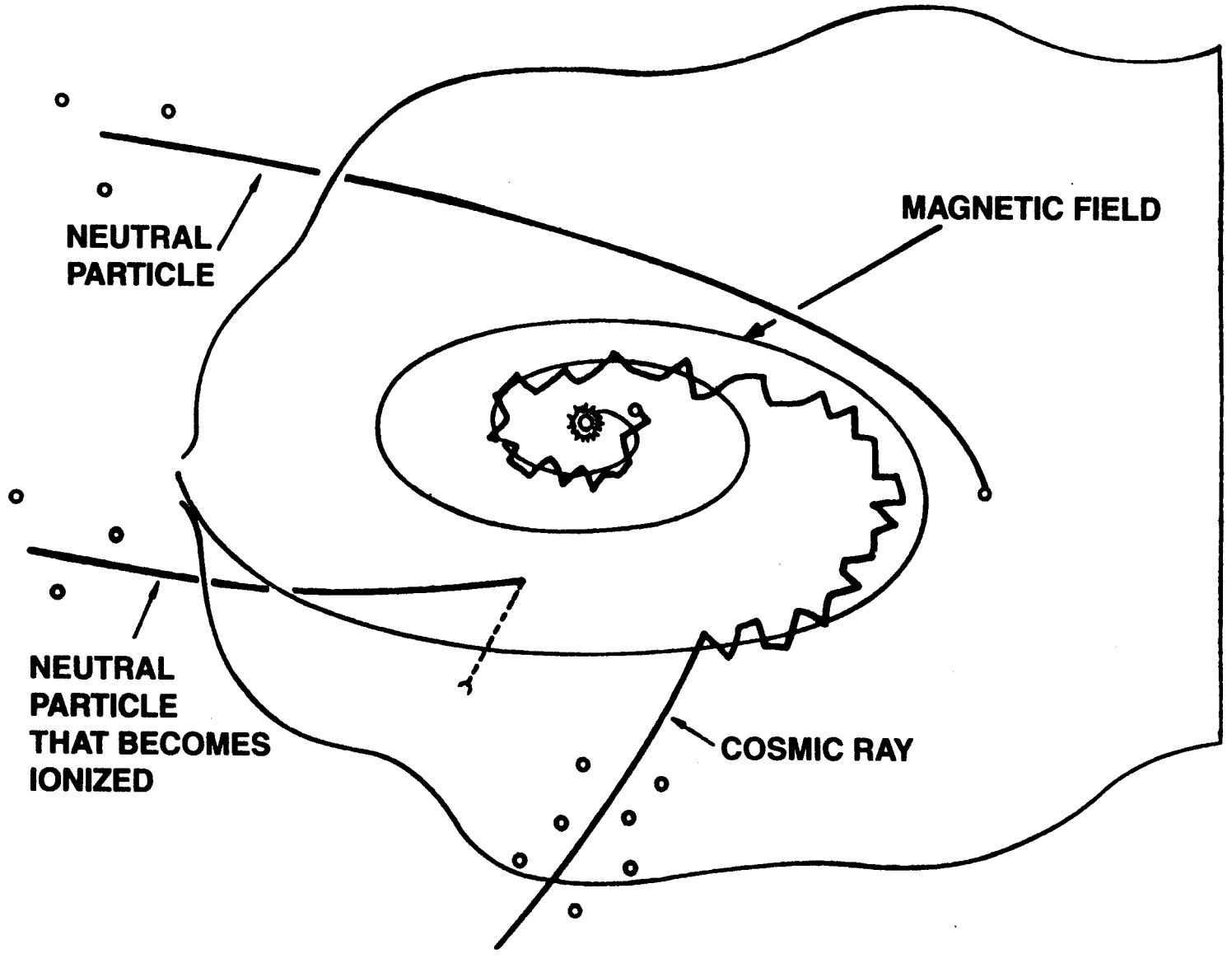
NEUTRAL
PARTICLE
MAGNETIC FIELD
NEUTRAL
PARTICLE
THAT BECOMES
IONIZED
COSMIC RAY

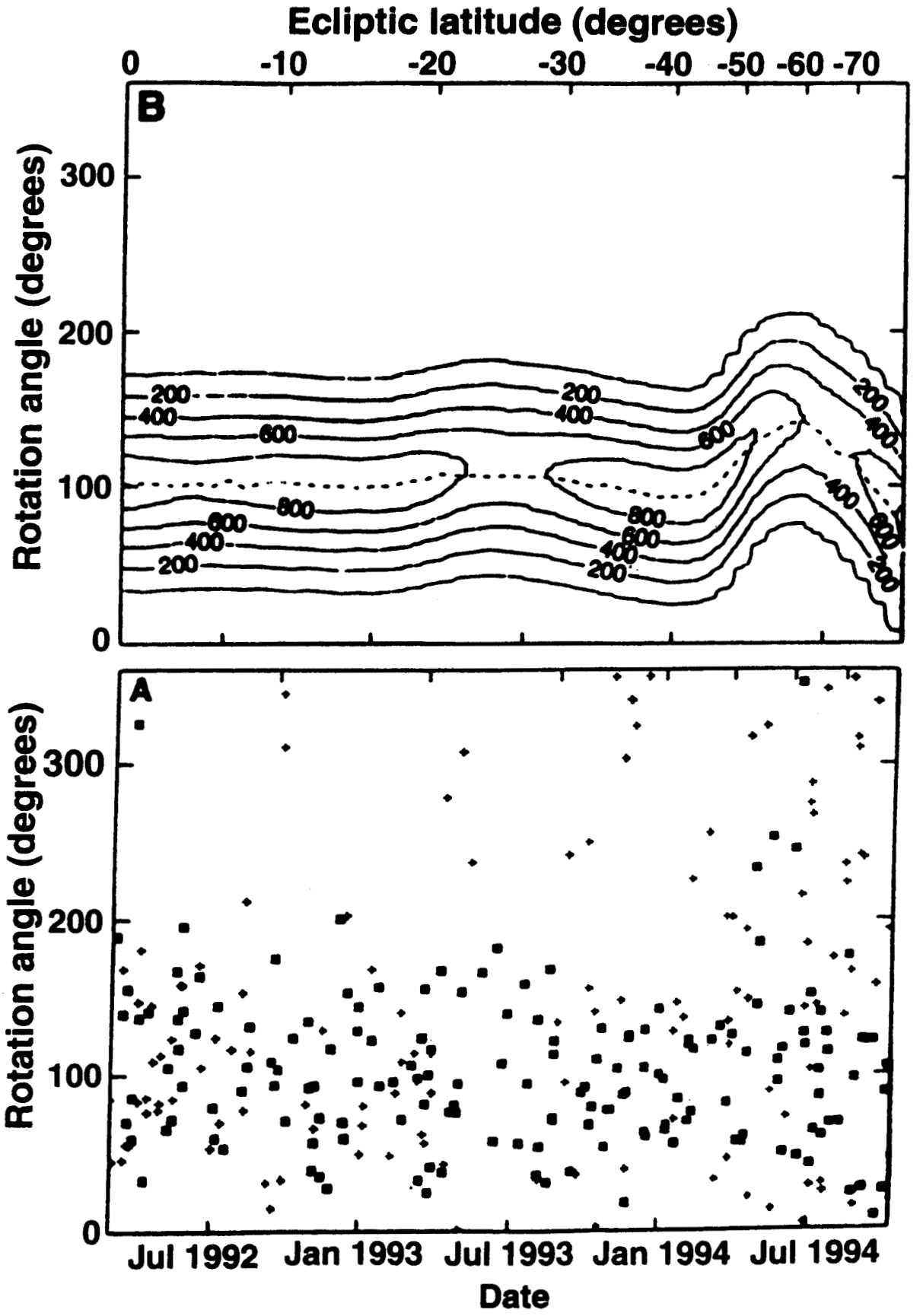
Ecliptic latitude (degrees)
0
-10
-20
-30
-40
-50
-60
-70
B
Rotation angle (degrees)
300
200
100
0
200
400
600
800
A
Jul 1992
Jan 1993
Jul 1993
Jan 1994
Jul 1994
Date

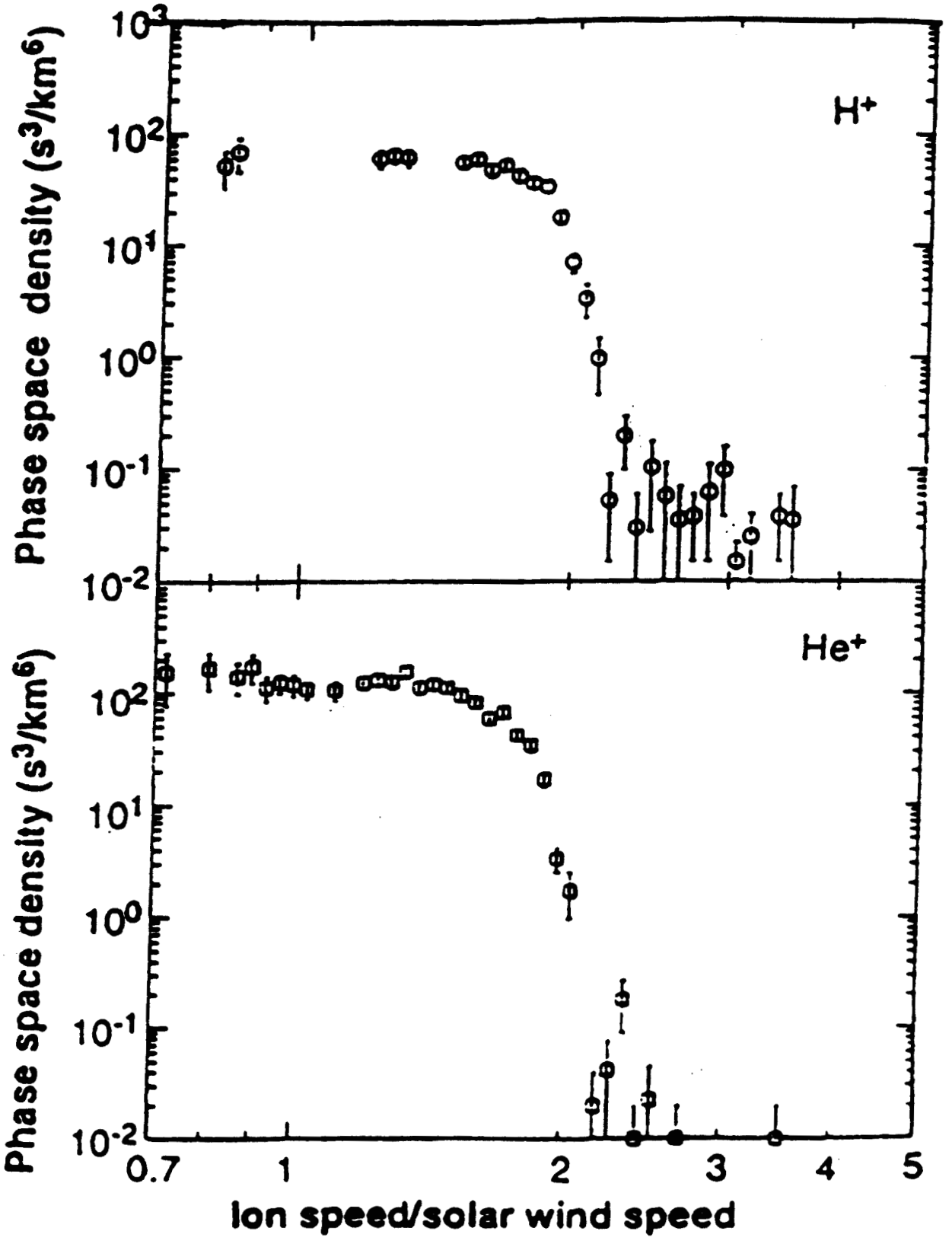
Phase space density (s³/km⁶)
H⁺
He⁺
Ion speed/solar wind speed
0.7
1
2
3
4
5

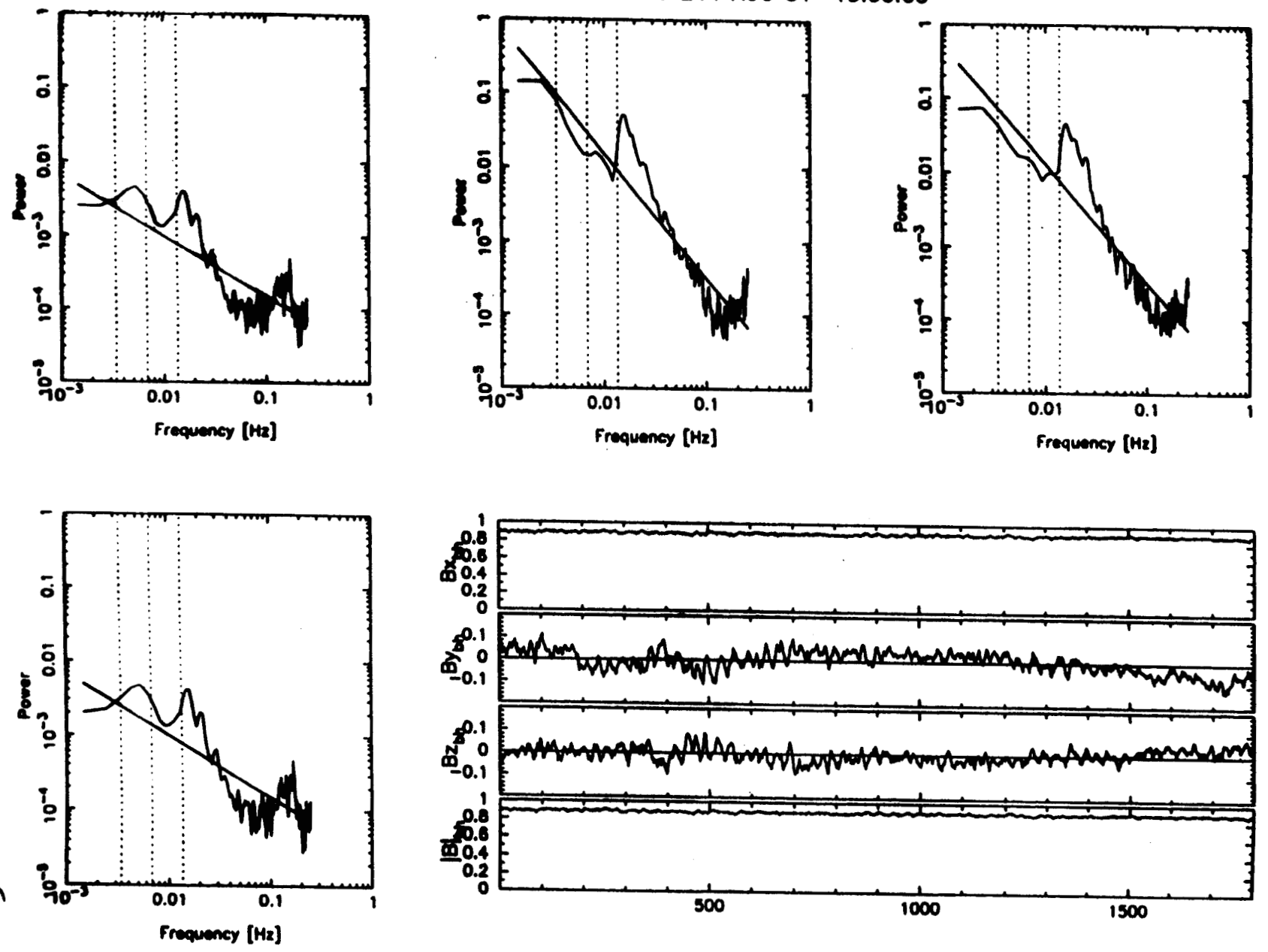
96 244 AUG 31 14:00:00.000 to 96 244 AUG 31 15:00:00
Power
Frequency [Hz]
Power
Frequency [Hz]
Power
Frequency [Hz]
Power
Frequency [Hz]
Bx
By
Bz
|B|
500
1000
1500

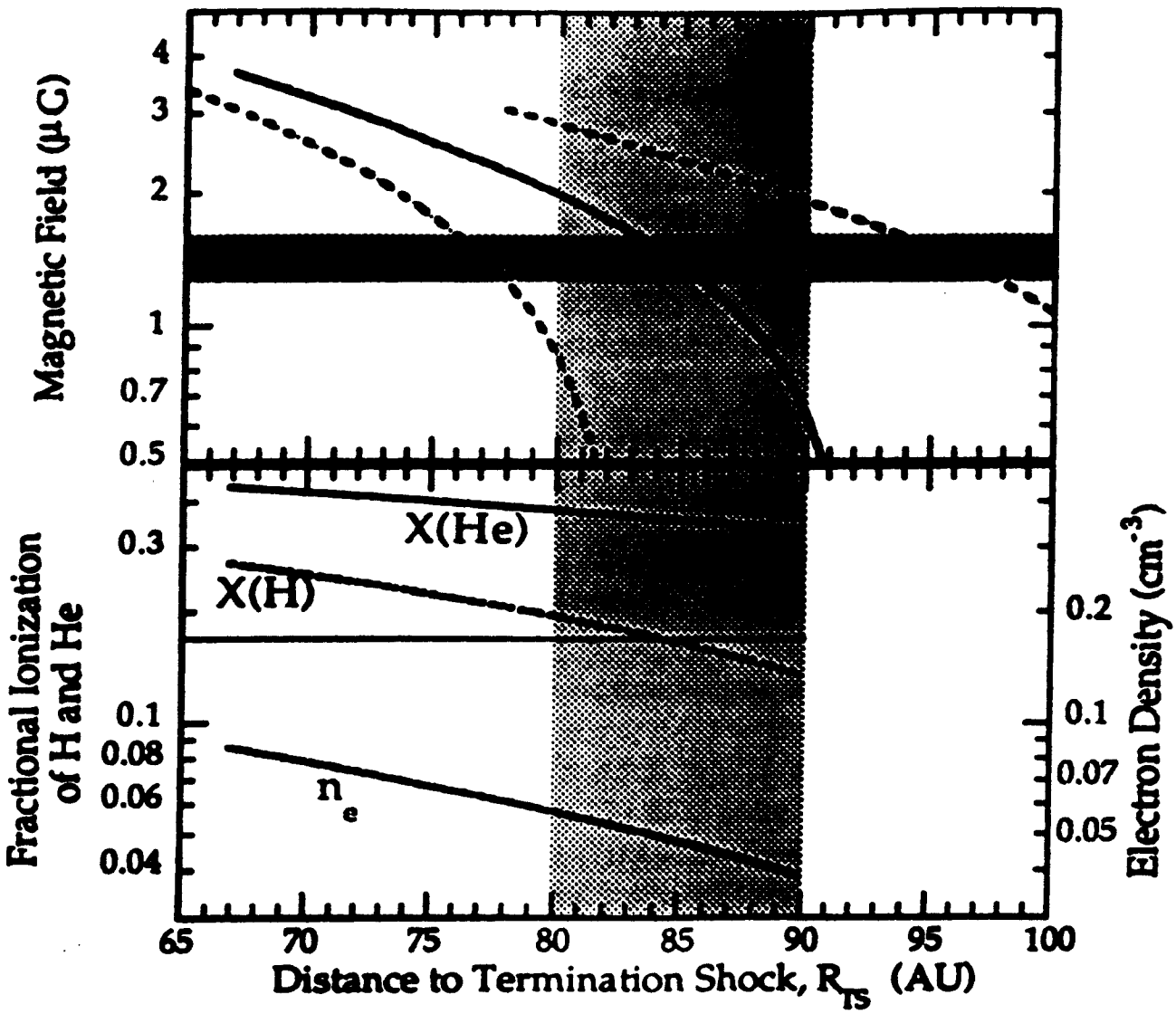
Magnetic Field (μG)
4
3
2
1
0.7
0.5
X(He)
X(H)
0.3
0.2
0.1
0.08
0.06
0.04
n_e
0.1
0.07
0.05
Fractional Ionization of H and He
Electron Density (cm^{-3})
65
70
75
80
85
90
95
100
Distance to Termination Shock, R_{TS} (AU)

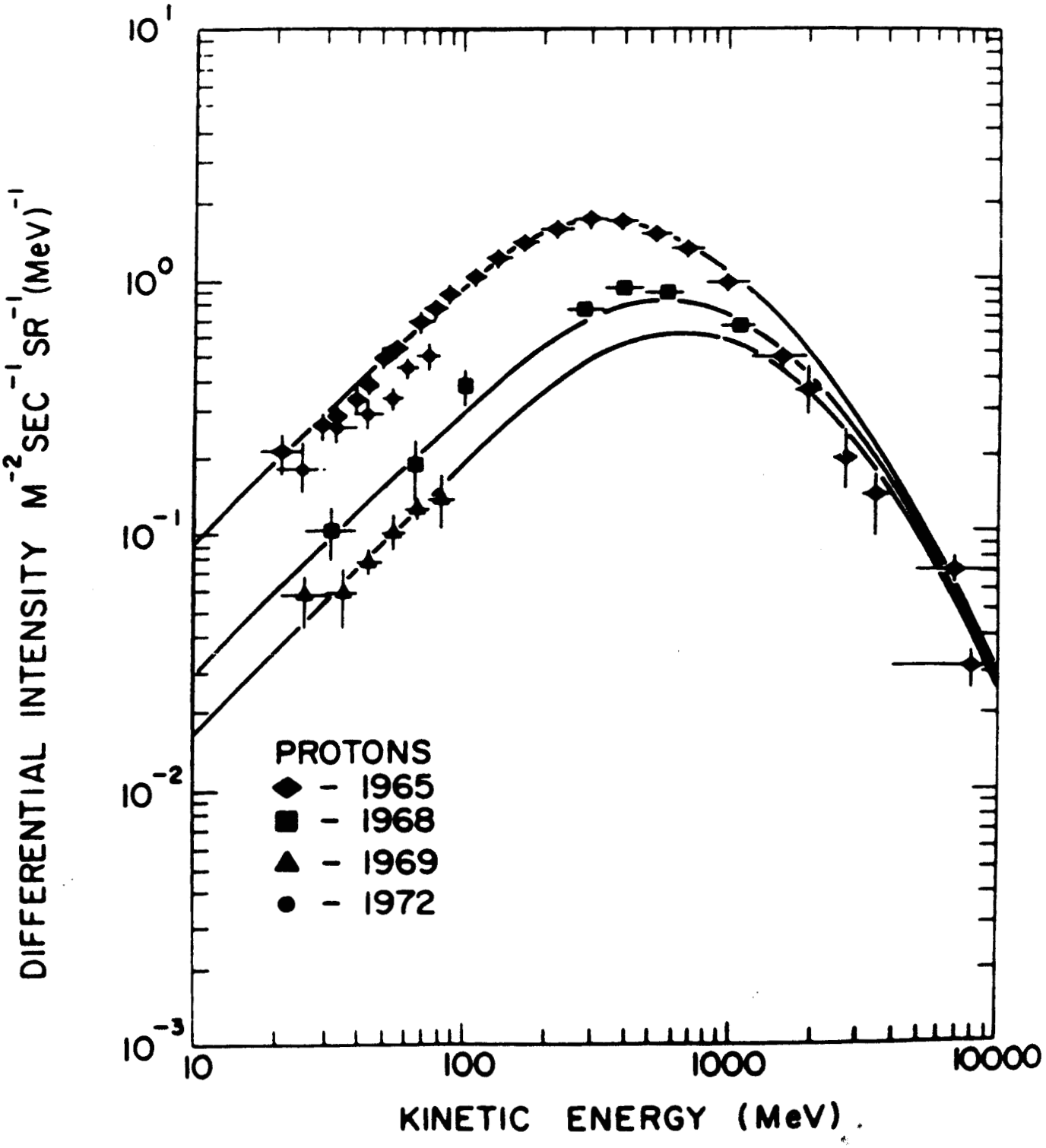
DIFFERENTIAL INTENSITY M^{-2}SEC^{-1}SR^{-1}(MeV)$^{-1}$
10^{1}
10^{0}
10^{-1}
10^{-2}
10^{-3}
PROTONS
◆ - 1965
■ - 1968
▲ - 1969
● - 1972
10
100
1000
10000
KINETIC ENERGY (MeV)

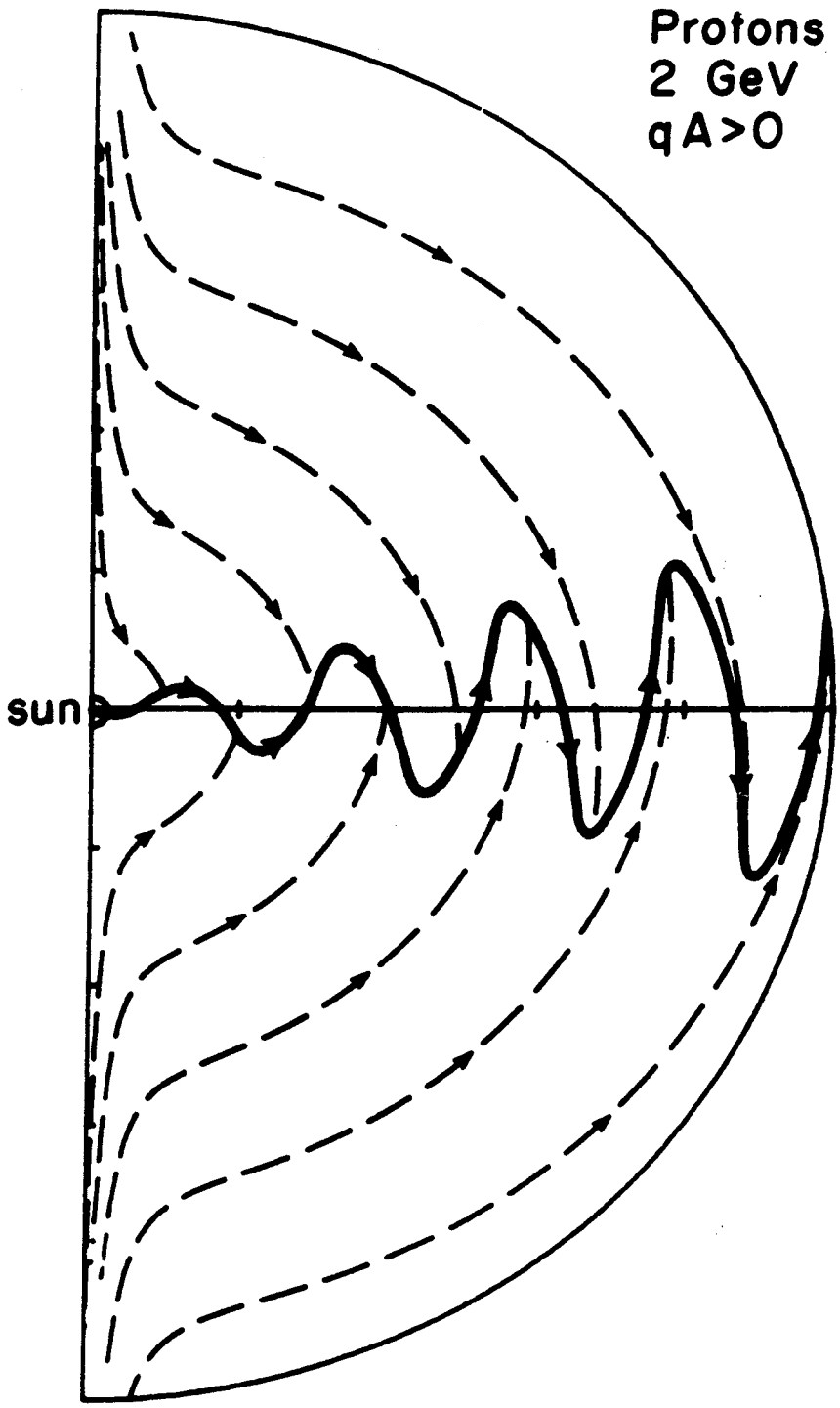
Protons
2 GeV
qA>0
sun

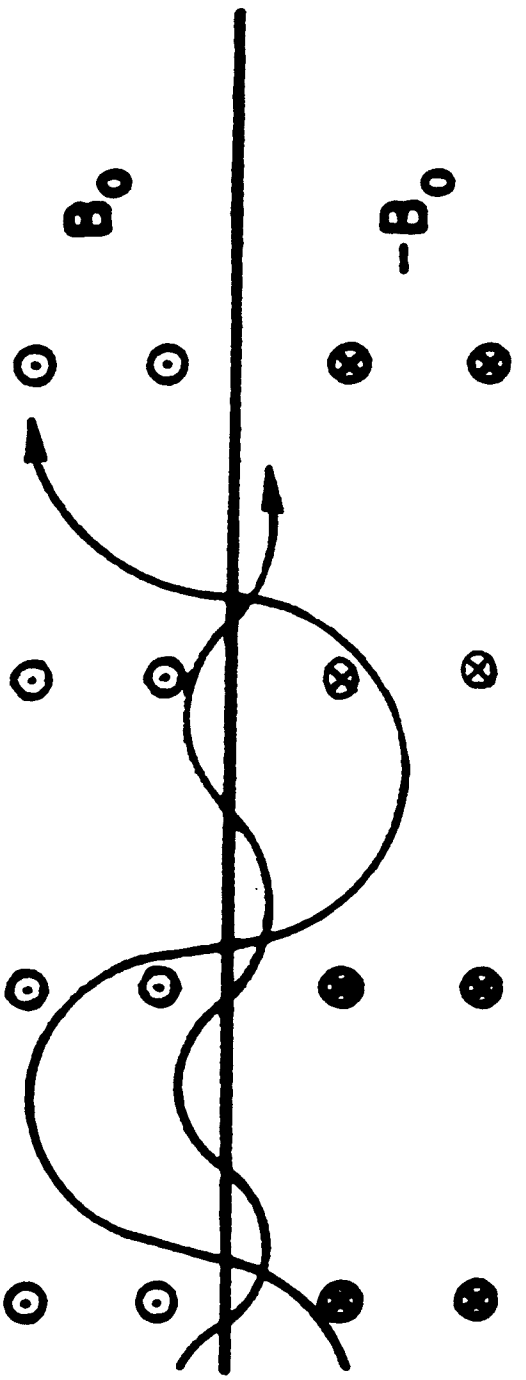
B_0
$-B_0$

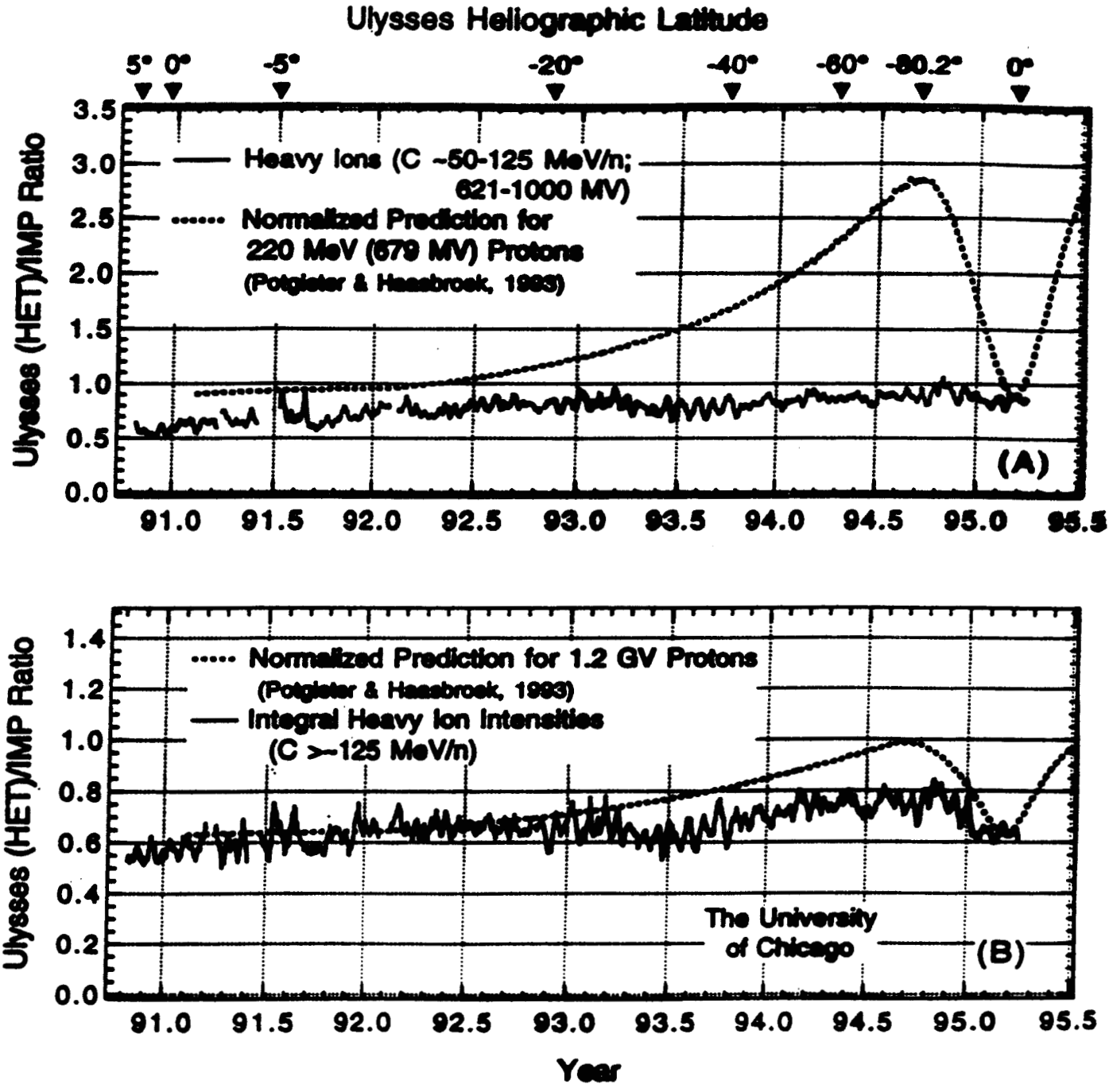
Ulysses Heliographic Latitude
5° 0° -5° -20° -40° -60° -80.2° 0°
Ulysses (HET)/IMP Ratio
Heavy Ions (C ~50-125 MeV/n; 621-1000 MV)
Normalized Prediction for 220 MeV (579 MV) Protons
(Potgieter & Haasbroek, 1993)
(A)
Normalized Prediction for 1.2 GV Protons
(Potgieter & Haasbroek, 1993)
Integral Heavy Ion Intensities (C >~125 MeV/n)
The University of Chicago
(B)
Year

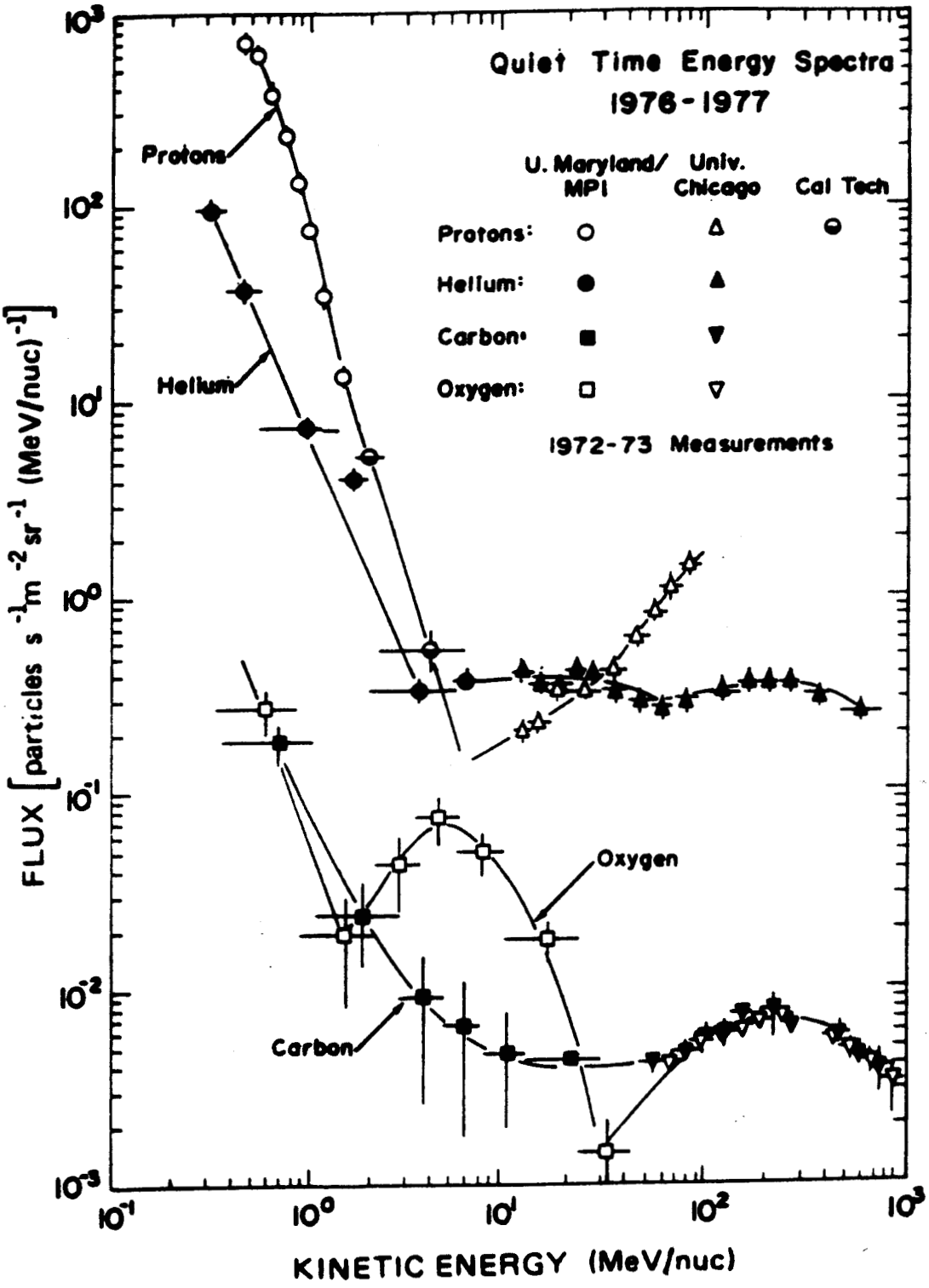
Quiet Time Energy Spectra
1976-1977
U. Maryland/ MPI
Univ. Chicago
Cal Tech
Protons:
Helium:
Carbon:
Oxygen:
1972-73 Measurements
Protons
Helium
Oxygen
Carbon
FLUX [particles s⁻¹m⁻²sr⁻¹ (MeV/nuc)⁻¹]
KINETIC ENERGY (MeV/nuc)

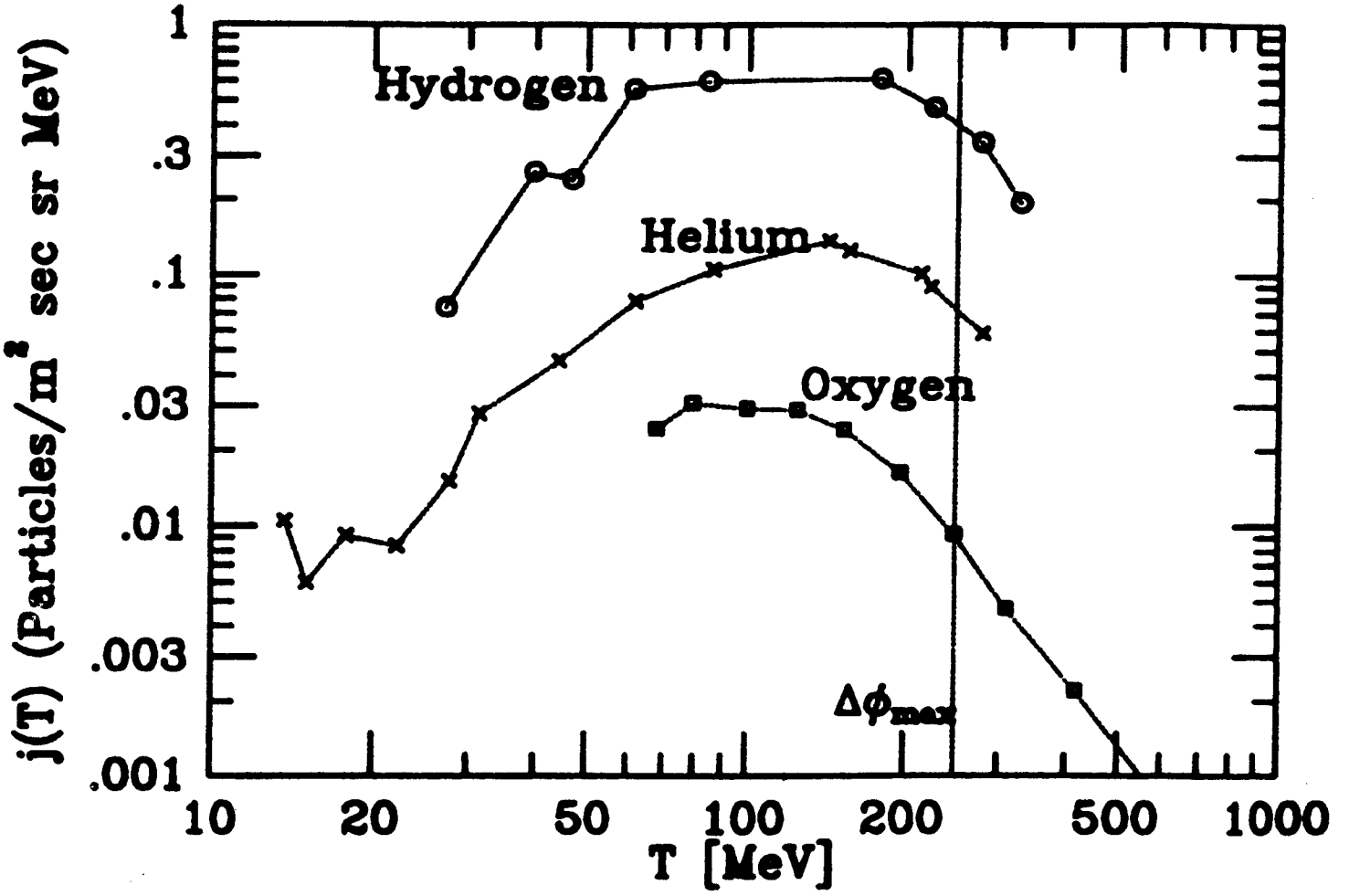
Hydrogen
Helium
Oxygen
$\Delta\phi_{max}$
j(T) (Particles/m² sec sr MeV)
T [MeV]
1
.3
.1
.03
.01
.003
.001
10
20
50
100
200
500
1000

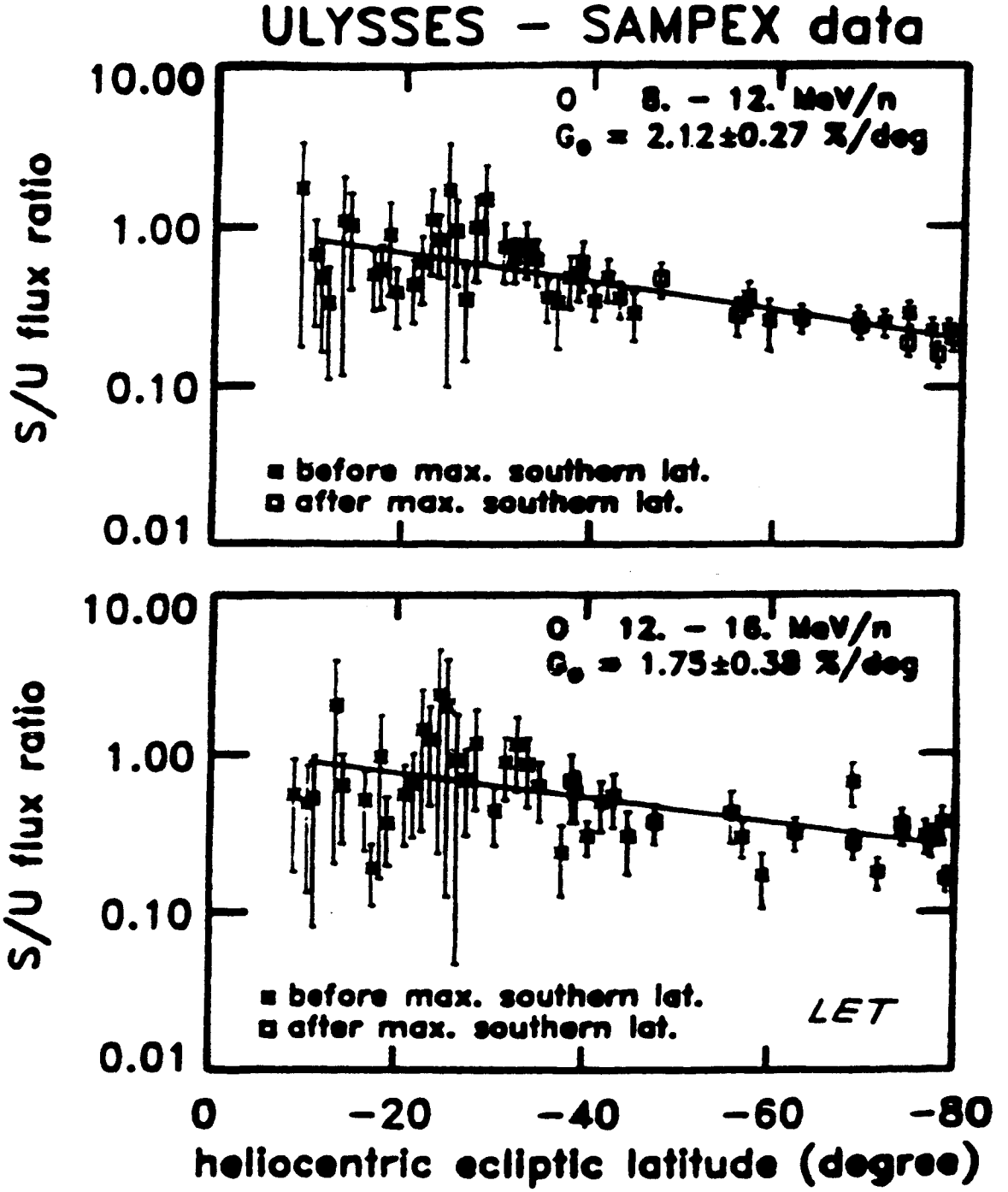
ULYSSES – SAMPEX data
O 8. – 12. MeV/n
G_θ = 2.12±0.27 %/deg
■ before max. southern lat.
□ after max. southern lat.
O 12. – 16. MeV/n
G_θ = 1.75±0.38 %/deg
■ before max. southern lat.
□ after max. southern lat.
LET
S/U flux ratio
10.00
1.00
0.10
0.01
0
−20
−40
−60
−80
heliocentric ecliptic latitude (degree)